1-12-2022

Electromagnetic Multi–Gaussian Speckle

Milo W. Hyde IV
Air Force Institute of Technology

Olga Korotkova
University of Miami

Recommended Citation

Hyde, M. W., & Korotkova, O. (2022). Electromagnetic Multi–Gaussian Speckle. Optics, 3(1), 19–34. https://doi.org/10.3390/opt3010003

optics

MDPI

Article

Electromagnetic Multi–Gaussian Speckle

Milo W. Hyde IV [1,*,†,‡] and Olga Korotkova [2,‡]

[1] Department of Engineering Physics, Air Force Institute of Technology, 2950 Hobson Way, Dayton, OH 45433, USA
[2] Department of Physics, University of Miami, 1320 Campo Sano Drive, Coral Gables, FL 33146, USA; o.korotkova@miami.edu
* Correspondence: milo.hyde@afit.edu
† The views expressed in this paper are those of the authors and do not reflect the official policy or position of the U.S. Air Force, the Department of Defense, or the U.S. Government.
‡ These authors contributed equally to this work.

Abstract: Generalizing our prior work on scalar multi-Gaussian (MG) distributed optical fields, we introduce the two-dimensional instantaneous electric-field vector whose components are jointly MG distributed. We then derive the single-point Stokes parameter probability density functions (PDFs) of MG-distributed light having an arbitrary degree and state of polarization. We show, in particular, that the intensity contrast of such a field can be tuned to values smaller or larger than unity. We validate our analysis by generating an example partially polarized MG field with a specified single-point polarization matrix using two different Monte Carlo simulation methods. We then compute the joint PDFs of the instantaneous field components and the Stokes parameter PDFs from the simulated MG fields, while comparing the results of both Monte Carlo methods to the corresponding theory. Lastly, we discuss the strengths, weaknesses, and applicability of both simulation methods in generating MG fields.

Keywords: partially polarized light; random light; speckle; statistical optics

Citation: Hyde, M.W., IV; Korotkova, O. Electromagnetic Multi–Gaussian Speckle. *Optics* **2022**, *3*, 19–34. https://doi.org/10.3390/opt3010003

Academic Editor: Thomas Seeger

Received: 3 December 2021
Accepted: 7 January 2022
Published: 12 January 2022

1. Introduction

Light speckle is one of the classic areas of study in statistical optics manifesting itself via spatial intensity randomization and being the consequence of field interference. Observed shortly after the invention of the laser, speckle has attracted the attention of the world's leading optical scientists. Speckle research began in the 1960s and 70s with the seminal works of Goodman and Dainty [1–4]. Based on physical arguments regarding its origins, the instantaneous electromagnetic field comprising speckle is traditionally assumed to be stationary and obey Gaussian statistics. As a result, the probability density functions (PDFs) of all physically meaningful polarization metrics—Stokes parameters [5–9], degree of polarization [10], polarization ellipse parameters [11]—have been derived in closed form. Moreover, with knowledge of the second-order, two-point correlation function of the source/scatterer, the various statistics of the Gaussian field can be examined on propagation/scattering [12,13]. In addition, the study of speckle has led to insights in singular optics on topics such as the nature and behavior of phase, polarization, and coherence vortices [14–19].

For a long time, speckle was considered to be a deleterious effect in coherent imaging systems, and multiple methods have been developed for its mitigation, i.e., reducing its contrast, including wavelength, angle, and polarization diversity (see Chapter 6 of Ref. [18] and Chapter 10 of Ref. [20]). In the past few years, there has been interest in engineered, non-Gaussian speckle for use in microscopy and imaging applications [21–23]. With these potential applications in mind, we recently presented a new random variable [termed multi-Gaussian (MG)] for modeling stochastic optical fields, whose PDF was an alternating series of weighted Gaussian PDFs [24]. The shape of the MG PDF could be varied from

cusped to flat-topped by changing the value of a single parameter M (related to the number of terms in the series)—$M < 1$ for cusped PDFs, $M = 1$ reduces to the Gaussian PDF, and $M > 1$ for flat-topped distributions. This feature of the MG PDF, being a suitable sum of Gaussian PDFs, made it possible and, indeed, very affordable, to derive, in closed form, the PDF of intensity for scalar MG-distributed fields and consequently, determine speckle moments such as the contrast. Because of the control over the PDF afforded by M, the speckle contrast could be varied over a wide range, making stochastic MG fields potentially useful in engineered speckle applications.

In this paper, we generalize our prior work on scalar MG light to electromagnetic two-dimensional fields, including all cases of partial polarization. We start with the derivation of the bivariate complex MG PDF for characterization of the two mutually orthogonal components of the instantaneous electric field. We then find the moments of partially polarized MG speckle, including the speckle contrast, before concluding the theoretical analysis with derivations of the instantaneous Stokes parameter PDFs. To validate our analysis, we generate, in simulation, realizations of a generic electromagnetic MG speckle field using two different approaches. We then compute joint PDFs of the electric field components and the Stokes parameter PDFs and compare them to the corresponding theory. Lastly, we conclude our paper with a brief summary of the key results.

2. Theory

2.1. Bivariate Complex MG PDF

Let us start with the multivariate complex Gaussian distribution introduced by Wooding and Goodman [25,26]. Here, we specialize its form to describe a zero-mean, circular-complex-Gaussian (CCG) distributed [18], two-dimensional, stochastic electromagnetic field:

$$p_{E_x,E_y}(E_x, E_y) = \frac{\exp\left(-\boldsymbol{E}^\dagger \mathbf{J}^{-1} \boldsymbol{E}\right)}{\pi^2 \det(\mathbf{J})}, \tag{1}$$

where † is the Hermitian adjoint (conjugate transpose), $\mathbf{J}$ is the polarization matrix (also known as the coherency matrix) [9,18,27–31], and $\boldsymbol{E} = \begin{bmatrix} E_x & E_y \end{bmatrix}^{\mathrm{T}}$ (superscript T is the transpose).

Following the analysis presented in Ref. [24], let the function f be

$$f(\boldsymbol{E}) = \frac{1}{\pi^2 \det(\mathbf{J})} \left\{ 1 - \left[1 - \exp\left(-\boldsymbol{E}^\dagger \mathbf{J}^{-1} \boldsymbol{E} \right) \right]^M \right\}, \tag{2}$$

where $M > 0$ is the shape parameter. Equation (2) can be written as a series by using Newton's generalization of the binomial theorem, namely,

$$f(\boldsymbol{E}) = \frac{1}{\pi^2 \det(\mathbf{J})} \sum_{m=1}^{\infty} \frac{(M)_m}{m!} (-1)^{m-1} \exp\left(-m \boldsymbol{E}^\dagger \mathbf{J}^{-1} \boldsymbol{E} \right), \tag{3}$$

where $(M)_m$ is the Pochhammer symbol (falling factorial). If M is an integer, the corresponding series is finite with all terms greater than M equal to zero. With some simple algebra, we can write Equation (3) as a weighted sum of complex Gaussian distribution functions [see Equation (1)], viz.,

$$f(\boldsymbol{E}) = \sum_{m=1}^{\infty} \frac{(M)_m}{m!} \frac{(-1)^{m-1}}{m^2} \frac{\exp\left[-\boldsymbol{E}^\dagger (\mathbf{J}/m)^{-1} \boldsymbol{E} \right]}{\pi^2 \det(\mathbf{J}/m)}. \tag{4}$$

To be a valid PDF, f must integrate to unity and be non-negative for all $\boldsymbol{E}$. The latter condition is clearly satisfied [see Equation (2)]; normalizing Equation (4) satisfies the former:

$$p^{\mathrm{MG}}_{E_x,E_y}(E_x, E_y) = \frac{f(\boldsymbol{E})}{\int_{\mathbb{C}} \int_{\mathbb{C}} f(\boldsymbol{E}) \mathrm{d}E_x \mathrm{d}E_y}, \tag{5}$$

where the integrals with respect to E_x and E_y, in both cases, are taken over the entire complex plane. The denominator in Equation (5) is

$$\begin{aligned}\int_{\mathbb{C}}\int_{\mathbb{C}} f(\boldsymbol{E})\mathrm{d}E_x\mathrm{d}E_y &= \sum_{m=1}^{\infty}\frac{(M)_m}{m!}\frac{(-1)^{m-1}}{m^2}\int_{\mathbb{C}}\int_{\mathbb{C}}\frac{\exp\left[-\boldsymbol{E}^{\dagger}(\mathbf{J}/m)^{-1}\boldsymbol{E}\right]}{\pi^2\det(\mathbf{J}/m)}\mathrm{d}E_x\mathrm{d}E_y \\ &= \sum_{m=1}^{\infty}\frac{(M)_m}{m!}\frac{(-1)^{m-1}}{m^2} \\ &= C_{3/2}(M),\end{aligned} \tag{6}$$

where the normalization constant $C_{3/2}(M)$ is consistent with the general definition of $C_n(M)$ used in Ref. [24], viz.,

$$C_n(M) = \sum_{m=1}^{\infty}\frac{(M)_m}{m!}\frac{(-1)^{m-1}}{m^n\sqrt{m}}. \tag{7}$$

The bivariate complex MG PDF is therefore

$$p^{\mathrm{MG}}_{E_x,E_y}(E_x,E_y) = \frac{1}{C_{3/2}(M)}\sum_{m=1}^{\infty}\frac{(M)_m}{m!}\frac{(-1)^{m-1}}{m^2}\frac{\exp\left[-\boldsymbol{E}^{\dagger}(\mathbf{J}/m)^{-1}\boldsymbol{E}\right]}{\pi^2\det(\mathbf{J}/m)}. \tag{8}$$

In the case of completely polarized light, $\mathbf{J}$ becomes singular and statistics must be computed by taking the limit as $\det(\mathbf{J}) \to 0$.

Before proceeding, we note that the bivariate complex MG PDF given in Equation (8) is not equal to the corresponding multivariate real MG PDF [Equation (30)] in Ref. [24]. In fact, when the number of random variables is greater than two, Equation (30) in Ref. [24] is an invalid PDF, as it is negative for certain parameter values. It is important to highlight, however, that the scalar MG speckle analysis in Ref. [24] used the bivariate real MG PDF, and is therefore still valid. This observation is of physical importance for possibly modeling three-dimensional electromagnetic MG speckle fields, i.e., fields having three non-trivial mutually orthogonal electric field components. Such fields appear in confocal microscopy within the focal regions of lenses [32], and in scanning microscopy in close proximity to sources or scatterers [33].

2.2. The MG Polarization Matrix and Speckle Contrast

The bivariate complex MG PDF in Equation (8) is expressed in terms of Gaussian moments, namely, the polarization matrix $\mathbf{J}$. Here, we derive the MG polarization matrix in terms of Gaussian $\mathbf{J}$. We then use this result to derive the contrast for electromagnetic MG speckle.

The polarization matrix $\mathbf{J}$ is defined as [9,18,27–31]

$$\mathbf{J} = \begin{bmatrix} J_{xx} & J_{xy} \\ J_{xy}^* & J_{yy} \end{bmatrix} = \begin{bmatrix} \left\langle |E_x|^2 \right\rangle & \left\langle E_x E_y^* \right\rangle \\ \left\langle E_x^* E_y \right\rangle & \left\langle |E_y|^2 \right\rangle \end{bmatrix}, \tag{9}$$

where the angular brackets are ensemble averages. We can compute the second-order field moments in Equation (9) quite easily using Equation (8). Indeed, because Equation (8) contains the bivariate complex Gaussian PDF, we see at once that the MG polarization matrix is

$$\mathbf{J}^{\mathrm{MG}} = \mathbf{J}\frac{1}{C_{3/2}(M)}\sum_{m=1}^{\infty}\frac{(M)_m}{m!}\frac{(-1)^{m-1}}{m^3} = \mathbf{J}\frac{C_{5/2}(M)}{C_{3/2}(M)}. \tag{10}$$

For future analysis, it will be convenient to define a symbol for the ratio of normalization constants. Let $\zeta_n(M)$ be

$$\zeta_n(M) = \frac{C_{3/2+n}(M)}{C_{3/2}(M)}, \tag{11}$$

such that, $C_{5/2}(M)/C_{3/2}(M) = \zeta_1(M)$. Since the (average) Stokes parameters are linear combinations of the polarization matrix elements [9,18,27–31], the MG Stokes parameters are

$$\left\langle S_i^{\mathrm{MG}} \right\rangle = \left\langle S_i^{\mathrm{G}} \right\rangle \zeta_1(M), \tag{12}$$

where $i = 0, 1, 2, 3$. Lastly, the degree of polarization $\mathcal{P}$, angle of polarization ψ, and ellipticity angle χ are

$$\begin{aligned} \mathcal{P} &= \sqrt{1 - 4\frac{\det(\mathbf{J})}{\mathrm{tr}^2(\mathbf{J})}} \\ \psi &= \frac{1}{2}\arctan\left(\frac{J_{xy} + J_{xy}^*}{J_{xx} - J_{yy}}\right) \\ \chi &= \frac{1}{2}\arcsin\left[\frac{\mathrm{j}\left(J_{xy} - J_{xy}^*\right)}{\mathcal{P}\,\mathrm{tr}(\mathbf{J})}\right], \end{aligned} \tag{13}$$

where $\mathrm{tr}(\mathbf{J}) = J_{xx} + J_{yy}$ is the trace of $\mathbf{J}$ [9,29–31,34,35]. Because of the ratios in these quantities, the MG polarization ellipse parameters are equal to their Gaussian counterparts. The same is also true for the normalized Stokes parameters $\langle s_i \rangle = \langle S_i \rangle / \langle S_0 \rangle$, where $i = 0, 1, 2, 3$, that are also frequently used.

Proceeding to the speckle contrast,

$$\mathcal{C} = \frac{\sqrt{\langle I^2 \rangle - \langle I \rangle^2}}{\langle I \rangle}, \tag{14}$$

where $I = |E_x|^2 + |E_y|^2$ is the instantaneous intensity [18,31]. We have already found the average intensity $\langle I \rangle$, namely,

$$\langle I \rangle = \mathrm{tr}\left(\mathbf{J}^{\mathrm{MG}}\right) = \mathrm{tr}(\mathbf{J})\zeta_1(M). \tag{15}$$

We can find the second-moment of intensity using Equation (8) and the Gaussian moment theorem [18,31]. First, $\langle I^2 \rangle$ is

$$\left\langle I^2 \right\rangle = \left\langle |E_x|^4 \right\rangle + \left\langle |E_y|^4 \right\rangle + 2\left\langle |E_x|^2 |E_y|^2 \right\rangle. \tag{16}$$

For Gaussian E_x and E_y, each one of these fourth-order moments simplifies into the sum of products of second-order moments. Because its PDF contains the Gaussian distribution function, a similar thing happens for MG-distributed fields. For example, the joint moment in Equation (16) becomes:

$$\begin{aligned} \left\langle |E_x|^2 |E_y|^2 \right\rangle = \frac{1}{C_{3/2}(M)} \sum_{m=1}^{\infty} \frac{(M)_m}{m!} \frac{(-1)^{m-1}}{m^2} \\ \int_{\mathbb{C}} \int_{\mathbb{C}} |E_x|^2 |E_y|^2 \frac{\exp\left[-\boldsymbol{E}^{\dagger}(\mathbf{J}/m)^{-1}\boldsymbol{E}\right]}{\pi^2 \det(\mathbf{J}/m)} \mathrm{d}E_x \mathrm{d}E_y. \end{aligned} \tag{17}$$

We can either evaluate the integrals directly or apply the Gaussian moment theorem to obtain

$$\begin{aligned}\left\langle |E_x|^2 |E_y|^2 \right\rangle &= \frac{1}{C_{3/2}(M)} \sum_{m=1}^{\infty} \frac{(M)_m}{m!} \frac{(-1)^{m-1}}{m^2} \left(\frac{J_{xx}}{m} \frac{J_{yy}}{m} + \frac{|J_{xy}|^2}{m^2} \right) \\ &= \left(J_{xx} J_{yy} + |J_{xy}|^2 \right) \zeta_2(M).\end{aligned} \tag{18}$$

The other moments in Equation (16) can be derived from this result:

$$\begin{aligned}\left\langle I^2 \right\rangle &= 2\zeta_2(M) \left(J_{xx}^2 + J_{yy}^2 + J_{xx} J_{yy} + |J_{xy}|^2 \right) \\ &= 2\zeta_2(M) \left[\mathrm{tr}^2(\mathbf{J}) - \det(\mathbf{J}) \right].\end{aligned} \tag{19}$$

Substituting Equations (15) and (19) into Equation (14) and simplifying yields

$$\mathcal{C} = \frac{\sqrt{\mathrm{tr}^2(\mathbf{J}) \left[2\zeta_2(M) - \zeta_1^2(M) \right] - 2\zeta_2(M) \det(\mathbf{J})}}{\zeta_1(M) \, \mathrm{tr}(\mathbf{J})}. \tag{20}$$

We can simplify this expression further using the definition for $\mathcal{P}$ given in Equation (13), i.e., $\det(\mathbf{J}) = \mathrm{tr}^2(\mathbf{J}) \left(1 - \mathcal{P}^2 \right) / 4$. Inserting this into Equation (20) and after some basic algebra, we obtain

$$\mathcal{C} = \frac{1}{\sqrt{2}} \frac{\sqrt{\zeta_2(M)(3 + \mathcal{P}^2) - 2\zeta_1^2(M)}}{\zeta_1(M)}. \tag{21}$$

It is evident from the above expression that the electromagnetic MG speckle contrast depends only on the degree of polarization $\mathcal{P}$ and is independent of the state of polarization (characterized by parameters ψ and χ) for any M. Equation (21) can be shown to vary between

$$\sqrt{\frac{3}{2} \frac{\zeta_2(M)}{\zeta_1^2(M)} - 1} \leq \mathcal{C} \leq \sqrt{2 \frac{\zeta_2(M)}{\zeta_1^2(M)} - 1} \tag{22}$$

for $\mathcal{P} = 0$ and $\mathcal{P} = 1$, respectively. If $M = 1$, Equation (21) simplifies to the contrast for electromagnetic Gaussian speckle given in Ref. [18], viz.,

$$\mathcal{C} = \sqrt{\frac{1 + \mathcal{P}^2}{2}}, \tag{23}$$

which is bounded between $1/\sqrt{2} \leq \mathcal{C} \leq 1$—the limits corresponding to unpolarized and polarized speckle, respectively.

Figure 1 shows plots of the electromagnetic MG speckle contrast versus the shape parameter M and degree of polarization $\mathcal{P}$. The left surface plot [Figure 1a] displays $\mathcal{C}$ for $M \leq 1$, while the right plot [Figure 1b] displays $\mathcal{C}$ for $M \geq 1$. The speckle contrast for partially polarized CCG electromagnetic fields is therefore the front-right and back-left surface edges in (a) and (b), respectively. All values of the contrast in (b) are $\mathcal{C} \leq 1$; $\mathcal{C} > 1$ can only occur when $M < 1$.

Figure 1c,d show the MG contrast as $M \to 0$ and $M \to \infty$, numerically computed (extrapolated), respectively. Furthermore, plotted on (c) and (d), for ease of comparison, is the Gaussian speckle contrast [see Equation (23)]. We estimated the speckle contrast as $M \to 0$ by evaluating Equation (21) from $M = 0.001$ to $M = 1$ and $\mathcal{P} = 0$ to $\mathcal{P} = 1$ in 500^2 equal steps across the two-dimensional space. We then found the coefficients of the following fourth-order polynomial that resulted in the best fit to the speckle contrast:

$$\mathcal{C}(M, \mathcal{P}) \approx \sum_{i=0}^{4} \sum_{j=0}^{4} a_{ij} M^i \mathcal{P}^j. \tag{24}$$

Lastly, we used Equation (24) to predict $\mathcal{C}$ at $M = 0$. We used a similar process to estimate $\mathcal{C}$ as $M \to \infty$. We first evaluated Equation (21) from $M = 50$ to $M = 1$ and $\mathcal{P} = 0$ to $\mathcal{P} = 1$ again in 500^2 equal steps. We then found the coefficients of the polynomial in Equation (24) that yielded the best fit to $\mathcal{C}$ when plotted versus $1/M$ and P. Lastly, we used the resulting polynomial to predict $\mathcal{C}$ when $1/M = 0$.

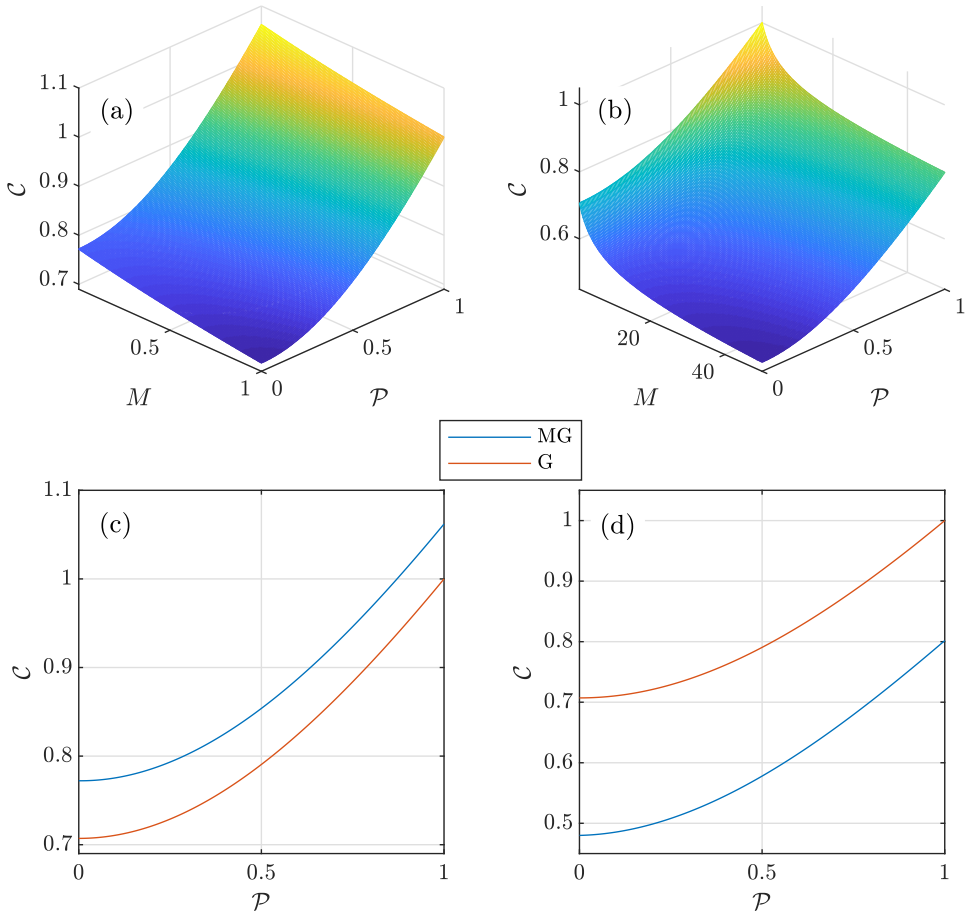

Figure 1. Contrast of partially polarized MG speckle versus shape parameter M and degree of polarization $\mathcal{P}$: (**a**) $M \leq 1$, (**b**) $M \geq 1$, (**c**) $M \to 0$, and (**d**) $M \to \infty$.

Summarizing the main results of this section, we state that electromagnetic MG speckle fields allow for fine control over the speckle contrast. The range of MG $\mathcal{C}$ is much larger than that of Gaussian speckle fields for the same value of $\mathcal{P}$, and the polarization state is unaffected.

2.3. Instantaneous Stokes Parameter PDFs for MG Speckle

Following the approach used by Brosseau et al. to derive the Stokes parameter PDFs for CCG electromagnetic fields [6,9], we first find the MG Stokes parameter characteristic functions using Equation (8). Then, we inverse Fourier transform the characteristic functions to find the PDFs.

2.3.1. S_0

Starting with S_0, the characteristic function is

$$\begin{aligned} \langle \exp(\mathrm{j}\omega S_0) \rangle &= \int_0^\infty \exp(\mathrm{j}\omega S_0) p_{S_0}(S_0) \mathrm{d}S_0 \\ &= \int_{\mathbb{C}} \int_{\mathbb{C}} \exp\left(\mathrm{j}\omega |E_x|^2\right) \exp\left(\mathrm{j}\omega |E_y|^2\right) p^{\mathrm{MG}}_{E_x,E_y}(E_x, E_y) \mathrm{d}E_x \mathrm{d}E_y. \end{aligned} \tag{25}$$

Substituting Equation (8) into Equation (25) and bringing the integrals inside the sum produces

$$\begin{aligned}\langle \exp(\mathrm{j}\omega S_0)\rangle = &\frac{1}{C_{3/2}(M)}\sum_{m=1}^{\infty}\frac{(M)_m}{m!}\frac{(-1)^{m-1}}{m^2}\\ &\frac{1}{\pi^2\det(\mathbf{J}/m)}\int_{\mathbb{C}}\int_{\mathbb{C}}\exp\left\{-\boldsymbol{E}^{\dagger}\left[(\mathbf{J}/m)^{-1}-\mathrm{j}\omega\mathbf{I}\right]\boldsymbol{E}\right\}\mathrm{d}E_x\mathrm{d}E_y,\end{aligned} \tag{26}$$

where $\mathbf{I}$ is the identity matrix. The above integrals evaluate to [26,36]

$$\int_{\mathbb{C}}\int_{\mathbb{C}}\exp\left\{-\boldsymbol{E}^{\dagger}\left[(\mathbf{J}/m)^{-1}-\mathrm{j}\omega\mathbf{I}\right]\boldsymbol{E}\right\}\mathrm{d}E_x\mathrm{d}E_y=\pi^2\det\left\{\left[(\mathbf{J}/m)^{-1}-\mathrm{j}\omega\mathbf{I}\right]^{-1}\right\}. \tag{27}$$

Substituting this into Equation (26) and simplifying using $\det(\mathbf{A}^{-1}) = 1/\det(\mathbf{A})$ and $\det(\mathbf{A})\det(\mathbf{B}) = \det(\mathbf{AB})$ yields the characteristic function for S_0:

$$\langle \exp(\mathrm{j}\omega S_0)\rangle = \frac{1}{C_{3/2}(M)}\sum_{m=1}^{\infty}\frac{(M)_m}{m!}\frac{(-1)^{m-1}}{m^2}\frac{1}{\det(\mathbf{I}-\mathrm{j}\omega\mathbf{J}/m)}. \tag{28}$$

The PDF for S_0 can be found by inverse Fourier transforming Equation (28), namely,

$$\begin{aligned}p_{S_0}(S_0) &= \frac{1}{2\pi}\int_{-\infty}^{\infty}\langle \exp(\mathrm{j}\omega S_0)\rangle\exp(-\mathrm{j}\omega S_0)\mathrm{d}\omega\\ &= \frac{1}{C_{3/2}(M)}\sum_{m=1}^{\infty}\frac{(M)_m}{m!}\frac{(-1)^{m-1}}{m^2}\frac{1}{2\pi}\int_{-\infty}^{\infty}\frac{\exp(-\mathrm{j}\omega S_0)}{\det(\mathbf{I}-\mathrm{j}\omega\mathbf{J}/m)}\mathrm{d}\omega.\end{aligned} \tag{29}$$

The determinant in the denominator of the integrand is easy to compute:

$$\det(\mathbf{I}-\mathrm{j}\omega\mathbf{J}/m) = 1-\mathrm{j}\frac{\omega}{m}\operatorname{tr}(\mathbf{J})-\frac{\omega^2}{m^2}\det(\mathbf{J}), \tag{30}$$

where $\operatorname{tr}(\mathbf{J}) = \langle S_0^{\mathrm{G}}\rangle$. The integrand in Equation (29) has two simple poles located at the roots of Equation (30):

$$\det(\mathbf{I}-\mathrm{j}\omega\mathbf{J}/m) = -\det(\mathbf{J}/m)\left[\omega+\mathrm{j}\frac{m}{2}\frac{\langle S_0^{\mathrm{G}}\rangle}{\det(\mathbf{J})}(1+\mathcal{P})\right]\left[\omega+\mathrm{j}\frac{m}{2}\frac{\langle S_0^{\mathrm{G}}\rangle}{\det(\mathbf{J})}(1-\mathcal{P})\right], \tag{31}$$

where $\mathcal{P}$ is the degree of polarization given in Equation (13). Both poles are in the lower-half complex ω plane. In addition, since S_0 is always positive, the integral in Equation (29) converges when the contour is closed in the lower-half ω plane. Applying Cauchy's integral theorem and formula, the integral in Equation (29) evaluates to

$$\begin{aligned}&\frac{1}{2\pi}\int_{-\infty}^{\infty}\frac{\exp(-\mathrm{j}\omega S_0)}{\det(\mathbf{I}-\mathrm{j}\omega\mathbf{J}/m)}\mathrm{d}\omega\\ &\quad=\frac{m}{\langle S_0^{\mathrm{G}}\rangle\mathcal{P}}\left\{\exp\left[-\frac{m}{2}\frac{\langle S_0^{\mathrm{G}}\rangle}{\det(\mathbf{J})}(1-\mathcal{P})S_0\right]-\exp\left[-\frac{m}{2}\frac{\langle S_0^{\mathrm{G}}\rangle}{\det(\mathbf{J})}(1+\mathcal{P})S_0\right]\right\}.\end{aligned} \tag{32}$$

Substituting $\det(\mathbf{J}) = \langle S_0^{\mathrm{G}}\rangle^2(1-\mathcal{P}^2)/4$ into the above expression and then inserting Equation (32) back into Equation (29) yields the final result:

$$\begin{aligned}p_{S_0}(S_0) = &\frac{1}{C_{3/2}(M)}\sum_{m=1}^{\infty}\frac{(M)_m}{m!}\frac{(-1)^{m-1}}{m}\\ &\frac{1}{\langle S_0^{\mathrm{G}}\rangle\mathcal{P}}\left\{\exp\left[-\frac{2mS_0}{\langle S_0^{\mathrm{G}}\rangle(1+\mathcal{P})}\right]-\exp\left[-\frac{2mS_0}{\langle S_0^{\mathrm{G}}\rangle(1-\mathcal{P})}\right]\right\}.\end{aligned} \tag{33}$$

2.3.2. S_1

The characteristic function for S_1 is

$$\begin{aligned}\langle \exp(\mathrm{j}\omega S_1)\rangle &= \int_{-\infty}^{\infty} \exp(\mathrm{j}\omega S_1) p_{S_1}(S_1)\mathrm{d}S_1 \\ &= \int_{\mathbb{C}}\int_{\mathbb{C}} \exp\left(\mathrm{j}\omega|E_x|^2\right)\exp\left(-\mathrm{j}\omega|E_y|^2\right) p^{\mathrm{MG}}_{E_x,E_y}(E_x,E_y)\mathrm{d}E_x\mathrm{d}E_y.\end{aligned} \tag{34}$$

Substituting Equation (8) into Equation (34) and bringing the integrals inside the sum produces

$$\begin{aligned}\langle \exp(\mathrm{j}\omega S_1)\rangle = \frac{1}{C_{3/2}(M)}\sum_{m=1}^{\infty}\frac{(M)_m}{m!}\frac{(-1)^{m-1}}{m^2} \\ \frac{1}{\pi^2\det(\mathbf{J}/m)}\int_{\mathbb{C}}\int_{\mathbb{C}}\exp\left(-\boldsymbol{E}^{\dagger}\left\{(\mathbf{J}/m)^{-1}-\mathrm{j}\omega\begin{bmatrix}1 & 0\\ 0 & -1\end{bmatrix}\right\}\boldsymbol{E}\right)\mathrm{d}E_x\mathrm{d}E_y.\end{aligned} \tag{35}$$

Referring back to Equation (27), Equation (35) simplifies to

$$\langle \exp(\mathrm{j}\omega S_1)\rangle = \frac{1}{C_{3/2}(M)}\sum_{m=1}^{\infty}\frac{(M)_m}{m!}\frac{(-1)^{m-1}}{m^2}\left\{\det\left(\mathbf{I}-\mathrm{j}\omega\frac{1}{m}\mathbf{J}\begin{bmatrix}1 & 0\\ 0 & -1\end{bmatrix}\right)\right\}^{-1}. \tag{36}$$

The PDF for S_1 is found by inverse Fourier transforming Equation (36):

$$\begin{aligned}p_{S_1}(S_1) &= \frac{1}{2\pi}\int_{-\infty}^{\infty}\langle \exp(\mathrm{j}\omega S_1)\rangle \exp(-\mathrm{j}\omega S_1)\mathrm{d}\omega \\ &= \frac{1}{C_{3/2}(M)}\sum_{m=1}^{\infty}\frac{(M)_m}{m!}\frac{(-1)^{m-1}}{m^2} \\ &\quad \frac{1}{2\pi}\int_{-\infty}^{\infty}\exp(-\mathrm{j}\omega S_1)\left\{\det\left(\mathbf{I}-\mathrm{j}\omega\frac{1}{m}\mathbf{J}\begin{bmatrix}1 & 0\\ 0 & -1\end{bmatrix}\right)\right\}^{-1}\mathrm{d}\omega,\end{aligned} \tag{37}$$

where

$$\begin{aligned}\det\left(\mathbf{I}-\mathrm{j}\omega\frac{1}{m}\mathbf{J}\begin{bmatrix}1 & 0\\ 0 & -1\end{bmatrix}\right) &= 1-\mathrm{j}\frac{\omega}{m}(J_{xx}-J_{yy})+\frac{\omega^2}{m^2}\det(\mathbf{J}) \\ &= \frac{\det(\mathbf{J})}{m^2}\left(\omega^2-\mathrm{j}\frac{m\langle S_1^{\mathrm{G}}\rangle}{\det(\mathbf{J})}\omega+\frac{m^2}{\det(\mathbf{J})}\right).\end{aligned} \tag{38}$$

Note that $J_{xx}-J_{yy}=\langle S_1^{\mathrm{G}}\rangle$. The integrand in Equation (37) has two simple poles at the roots of Equation (38), viz.,

$$\begin{aligned}&\det\left(\mathbf{I}-\mathrm{j}\omega\frac{1}{m}\mathbf{J}\begin{bmatrix}1 & 0\\ 0 & -1\end{bmatrix}\right) \\ &= \frac{\det(\mathbf{J})}{m^2}\prod_{+,-}\left\{\omega-\mathrm{j}\frac{m}{2\det(\mathbf{J})}\left[\left\langle S_1^{\mathrm{G}}\right\rangle \pm \sqrt{\langle S_1^{\mathrm{G}}\rangle^2+4\det(\mathbf{J})}\right]\right\}.\end{aligned} \tag{39}$$

Since $\det(\mathbf{J})\geq 0$ [9,18,27–31], the "plus" root is always in the upper-half ω plane, while the "minus" root is always in the lower-half plane. If $S_1<0$, the integral in Equation (37) converges when the contour is closed in the upper-half plane and only the "plus" root contributes—vice versa, if $S_1>0$. The two results can be combined to produce

$$\begin{aligned}&\frac{1}{2\pi}\int_{-\infty}^{\infty}\exp(-\mathrm{j}\omega S_1)\left\{\det\left(\mathbf{I}-\mathrm{j}\omega\frac{1}{m}\mathbf{J}\begin{bmatrix}1&0\\0&-1\end{bmatrix}\right)\right\}^{-1}\mathrm{d}\omega\\&\quad=\frac{m}{\sqrt{\langle S_1^{\mathrm{G}}\rangle^2+4\det(\mathbf{J})}}\exp\left\{-\frac{m|S_1|}{2\det(\mathbf{J})}\left[\sqrt{\langle S_1^{\mathrm{G}}\rangle^2+4\det(\mathbf{J})}-\mathrm{sgn}(S_1)\left\langle S_1^{\mathrm{G}}\right\rangle\right]\right\},\end{aligned}\tag{40}$$

where $\mathrm{sgn}(x)$ is the signum function. Substituting this into Equation (37) and using $\det(\mathbf{J})=\langle S_0^{\mathrm{G}}\rangle^2(1-\mathcal{P}^2)/4$ yields the following for p_{S_1}:

$$\begin{aligned}p_{S_1}(S_1)=&\frac{1}{C_{3/2}(M)}\sum_{m=1}^{\infty}\frac{(M)_m}{m!}\frac{(-1)^{m-1}}{m}\left[\left\langle S_0^{\mathrm{G}}\right\rangle^2\left(1-\mathcal{P}^2\right)+\left\langle S_1^{\mathrm{G}}\right\rangle^2\right]^{-1/2}\\&\exp\left\{-\frac{2m|S_1|}{\langle S_0^{\mathrm{G}}\rangle^2(1-\mathcal{P}^2)}\left[\sqrt{\langle S_0^{\mathrm{G}}\rangle^2(1-\mathcal{P}^2)+\langle S_1^{\mathrm{G}}\rangle^2}-\mathrm{sgn}(S_1)\left\langle S_1^{\mathrm{G}}\right\rangle\right]\right\}.\end{aligned}\tag{41}$$

2.3.3. S_2 and S_3

The process for finding the PDFs of S_2 and S_3 is the same as above. Jumping ahead to the final expressions for the characteristic functions,

$$\begin{aligned}\langle\exp(\mathrm{j}\omega S_2)\rangle&=\frac{1}{C_{3/2}(M)}\sum_{m=1}^{\infty}\frac{(M)_m}{m!}\frac{(-1)^{m-1}}{m^2}\left\{\det\left(\mathbf{I}-\mathrm{j}\omega\frac{1}{m}\mathbf{J}\begin{bmatrix}0&1\\1&0\end{bmatrix}\right)\right\}^{-1}\\\langle\exp(\mathrm{j}\omega S_3)\rangle&=\frac{1}{C_{3/2}(M)}\sum_{m=1}^{\infty}\frac{(M)_m}{m!}\frac{(-1)^{m-1}}{m^2}\left\{\det\left(\mathbf{I}+\omega\frac{1}{m}\mathbf{J}\begin{bmatrix}0&-1\\1&0\end{bmatrix}\right)\right\}^{-1}.\end{aligned}\tag{42}$$

The determinants evaluate to

$$\begin{aligned}\det\left(\mathbf{I}-\mathrm{j}\omega\frac{1}{m}\mathbf{J}\begin{bmatrix}0&1\\1&0\end{bmatrix}\right)&=1-\mathrm{j}\frac{\omega}{m}\left(J_{xy}+J_{xy}^*\right)+\frac{\omega^2}{m^2}\det(\mathbf{J})\\\det\left(\mathbf{I}+\omega\frac{1}{m}\mathbf{J}\begin{bmatrix}0&-1\\1&0\end{bmatrix}\right)&=1+\frac{\omega}{m}\left(J_{xy}-J_{xy}^*\right)+\frac{\omega^2}{m^2}\det(\mathbf{J}),\end{aligned}\tag{43}$$

where $J_{xy}+J_{xy}^*=\langle S_2^{\mathrm{G}}\rangle$ and $J_{xy}-J_{xy}^*=-\mathrm{j}\langle S_3^{\mathrm{G}}\rangle$. Substituting these into Equation (42), we see at once that the characteristic functions for S_2 and S_3 have the same form as Equation (36). Therefore, the PDFs for S_2 and S_3 have the same form as Equation (41). Consequently, we can combine the S_1, S_2, and S_3 PDFs into a single expression:

$$\begin{aligned}p_{S_i}(S_i)=&\frac{1}{C_{3/2}(M)}\sum_{m=1}^{\infty}\frac{(M)_m}{m!}\frac{(-1)^{m-1}}{m}\left[\left\langle S_0^{\mathrm{G}}\right\rangle^2\left(1-\mathcal{P}^2\right)+\left\langle S_i^{\mathrm{G}}\right\rangle^2\right]^{-1/2}\\&\exp\left\{-\frac{2m|S_i|}{\langle S_0^{\mathrm{G}}\rangle^2(1-\mathcal{P}^2)}\left[\sqrt{\langle S_0^{\mathrm{G}}\rangle^2(1-\mathcal{P}^2)+\langle S_i^{\mathrm{G}}\rangle^2}-\mathrm{sgn}(S_i)\left\langle S_i^{\mathrm{G}}\right\rangle\right]\right\},\end{aligned}\tag{44}$$

where $i=1,2,3$. Figures 2 and 3 show the PDFs of S_0 [Equation (33)] and S_i [Equation (44)] for various values of M and three values of $\mathcal{P}$. For these plots, $\langle S_0^{\mathrm{G}}\rangle=1$, such that $\langle S_i^{\mathrm{G}}\rangle=\mathcal{P}$. The $M=1$ curves are equal to the Stokes parameter PDFs for CCG electromagnetic fields in Refs. [5–9,18].

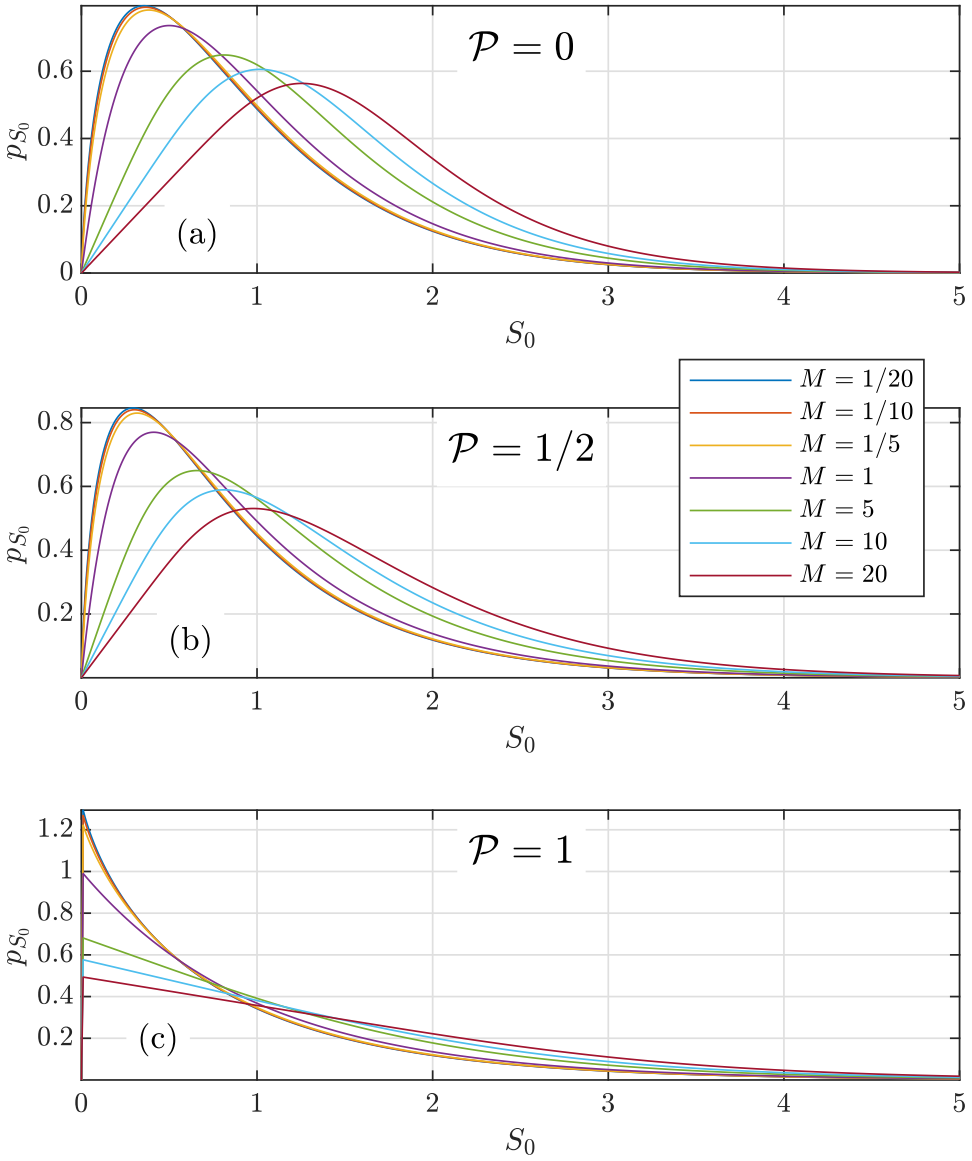

Figure 2. PDF of S_0 p_{S_0} [Equation (33)] for various values of M: (**a**) $\mathcal{P} = 0$, (**b**) $\mathcal{P} = 1/2$, and (**c**) $\mathcal{P} = 1$.

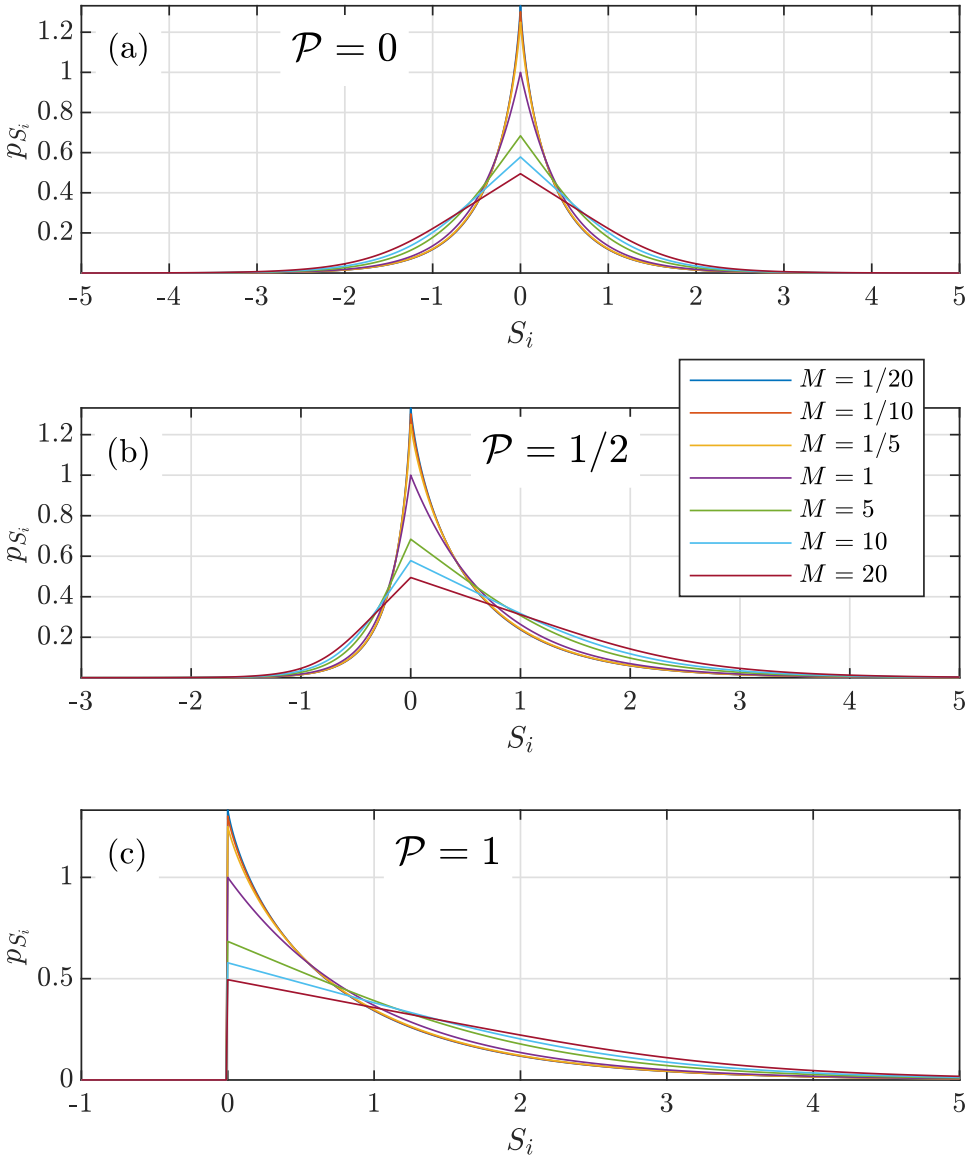

Figure 3. PDF of S_i p_{S_i} [Equation (44)] for various values of M: (**a**) $\mathcal{P} = 0$, (**b**) $\mathcal{P} = 1/2$, and (**c**) $\mathcal{P} = 1$.

3. Simulation

To validate the analysis of the previous section, we performed simulations where we created partially polarized MG speckle with a specific **J**. In these simulations, we used grids that were 256 points per side with a side-length equal to 1 m. We generated 500 MG speckle fields with shape parameter $M = 25$ and **J**

$$\mathbf{J} = \begin{bmatrix} 1 & 0.2\exp(\mathrm{j}\pi/3) \\ 0.2\exp(-\mathrm{j}\pi/3) & 0.6 \end{bmatrix} = \begin{bmatrix} 1.0000 & 0.1000 + \mathrm{j}0.1732 \\ 0.1000 - \mathrm{j}0.1732 & 0.6000 \end{bmatrix}. \quad (45)$$

The corresponding polarization ellipse parameters were

$$\begin{bmatrix} \mathcal{P} & \psi & \chi \end{bmatrix} = \begin{bmatrix} 0.3536 & 0.2318 & -0.3295 \end{bmatrix}. \quad (46)$$

From the 500 realizations of 256×256 MG E_x and E_y, we computed 6 joint field PDFs (every combination of the real and imaginary parts of E_x and E_y), the 4 Stokes parameter PDFs, the polarization matrix **J**, and the speckle contrast.

We generated the MG speckle fields using two approaches having contrasting strengths and weaknesses. For the first, we used rejection sampling (RS) [37], which produced E_x and E_y with the correct statistics described by Equation (8). However, using this approach,

both E_x and E_y were spatially "white," i.e., delta-correlated, and therefore did not have realistic speckle sizes. Note that it is theoretically possible to generate MG E_x and E_y, with physical speckle sizes, using RS. Yet, the computational cost to do so is immense, thereby making it practically impossible. For example, to generate an MG E_x with realistic speckle sizes would require rejection sampling a multivariate PDF with 256^2 dimensions. For the second synthesis approach, we used the normal-to-anything (NORTA) method [38–42], which efficiently generated E_x and E_y with realistic speckle sizes and the proper marginal (i.e., p_{E_x} and p_{E_y}) PDFs. Although NORTA did produce E_x and E_y with the correct average cross-correlation, the NORTA E_x and E_y did not have the correct joint PDF [Equation (8)], in contrast to RS. Results from both methods are presented and discussed below.

Figure 4 shows example RS and NORTA E_x realizations. The columns, from left to right, show the magnitude and phase of E_x; the rows, from top to bottom, show the RS and NORTA E_x, respectively. As discussed in the previous paragraph, the RS field realization [(a) and (b)] is essentially "white," with a speckle size approximately equal to the diameter of a pixel. In contrast, the NORTA realization [(c) and (d)] has a realistic speckle size, which can easily be controlled.

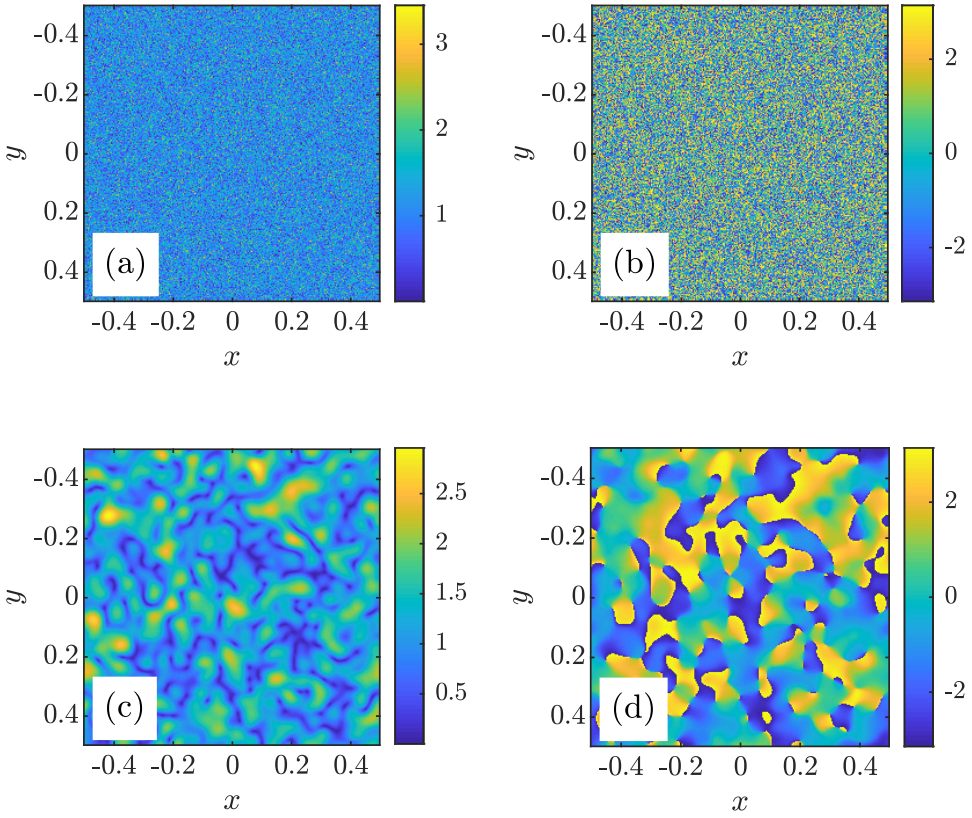

Figure 4. Rejection sampling (RS) and normal to anything (NORTA) E_x realizations: (**a**) RS $|E_x|$, (**b**) RS $\arg(E_x)$, (**c**) NORTA $|E_x|$, and (**d**) NORTA $\arg(E_x)$.

Figures 5 and 6 show the field and Stokes parameter PDF results, respectively. Figure 5 is organized such that the joint field PDFs are along the rows and the theoretical, RS, and NORTA PDFs are along the columns. We have labeled the rows and columns to aid the reader. In addition, the theoretical, RS, and NORTA PDF images in each row are encoded using the same color scales defined by the color bars at rows' end. Figure 6 displays, in four subfigures, the theoretical, RS, and NORTA Stokes parameter PDFs plotted together for ease of comparison.

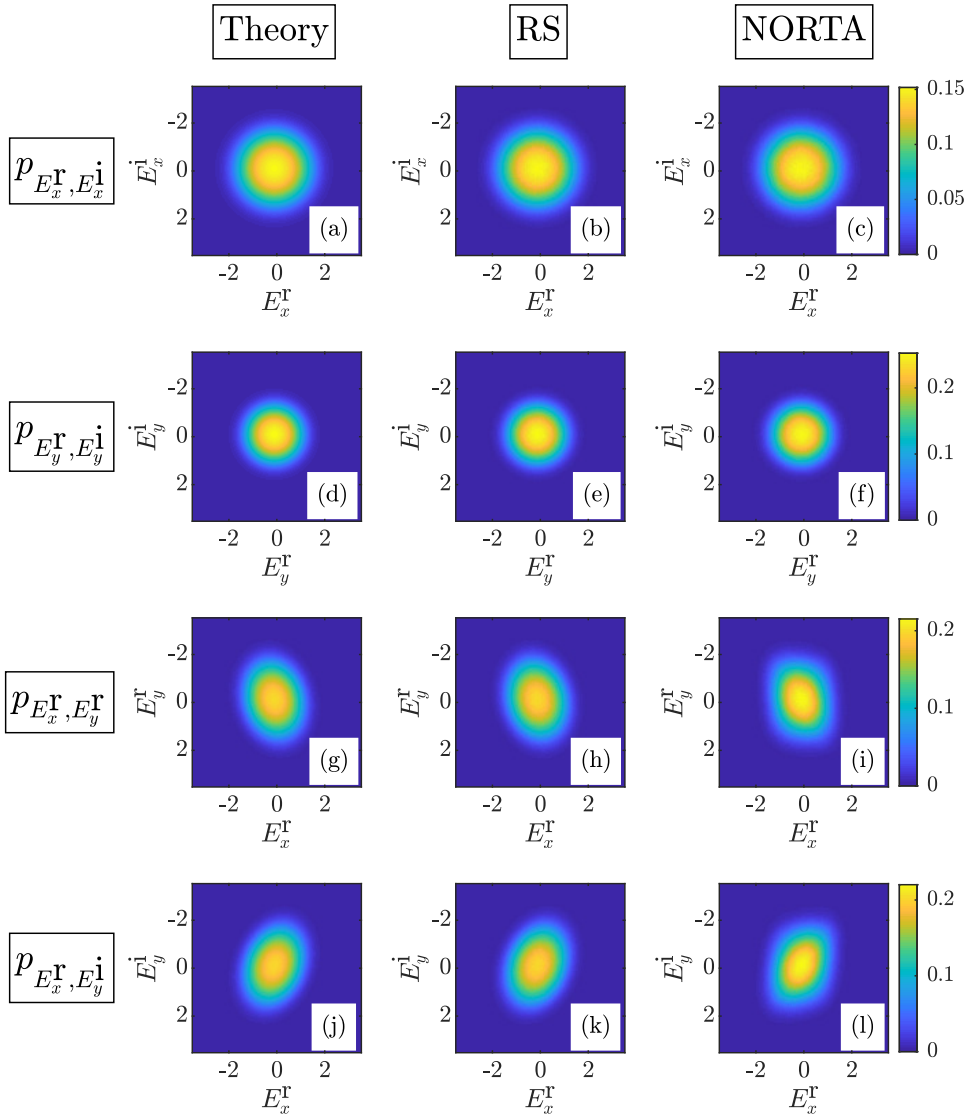

Figure 5. Joint PDFs of E_x and E_y: (**a**–**c**) theory, RS, NORTA $p_{E_x^{\mathrm{r}},E_x^{\mathrm{i}}}$, (**d**–**f**) theory, RS, NORTA $p_{E_y^{\mathrm{r}},E_y^{\mathrm{i}}}$, (**g**–**i**) theory, RS, NORTA $p_{E_x^{\mathrm{r}},E_y^{\mathrm{r}}}$, and (**j**–**l**) theory, RS, NORTA $p_{E_x^{\mathrm{r}},E_y^{\mathrm{i}}}$.

In all cases, the RS results are in excellent agreement with theory. On the other hand and as discussed above, NORTA generates E_x and E_y with the correct marginal statistics [Figure 5c,f], but inaccurate joint statistics [Figure 5i,l]. The inaccurate joint PDFs in (i) and (l) lead to discrepancies in the Stokes parameter PDFs in Figure 6 and consequently, to an incorrect speckle contrast—$\mathcal{C}^{\mathrm{thy}} = 0.5572$, $\mathcal{C}^{\mathrm{RS}} = 0.5575$, and $\mathcal{C}^{\mathrm{NORTA}} = 0.6173$. It should be mentioned however, that NORTA does generate E_x and E_y with the correct average cross-correlation. The polarization matrices for both RS and NORTA were

$$\begin{aligned} \mathbf{J}^{\mathrm{RS}} &= \begin{bmatrix} 1.0000 & 0.1000 + \mathrm{j}0.1731 \\ 0.1000 - \mathrm{j}0.1731 & 0.5999 \end{bmatrix} \\ \mathbf{J}^{\mathrm{NORTA}} &= \begin{bmatrix} 1.0004 & 0.1020 + \mathrm{j}0.1721 \\ 0.1020 - \mathrm{j}0.1721 & 0.5989 \end{bmatrix}, \end{aligned} \tag{47}$$

which matched the desired $\mathbf{J}$ [see Equation (45)] to the third decimal place. The corresponding polarization ellipse parameters were

$$\begin{aligned} \begin{bmatrix} \mathcal{P}^{\mathrm{RS}} & \psi^{\mathrm{RS}} & \chi^{\mathrm{RS}} \end{bmatrix} &= \begin{bmatrix} 0.3535 & 0.2318 & -0.3294 \end{bmatrix} \\ \begin{bmatrix} \mathcal{P}^{\mathrm{NORTA}} & \psi^{\mathrm{NORTA}} & \chi^{\mathrm{NORTA}} \end{bmatrix} &= \begin{bmatrix} 0.3544 & 0.2350 & -0.3262 \end{bmatrix}, \end{aligned} \tag{48}$$

which also were a good match to theory (see Equation (46)).

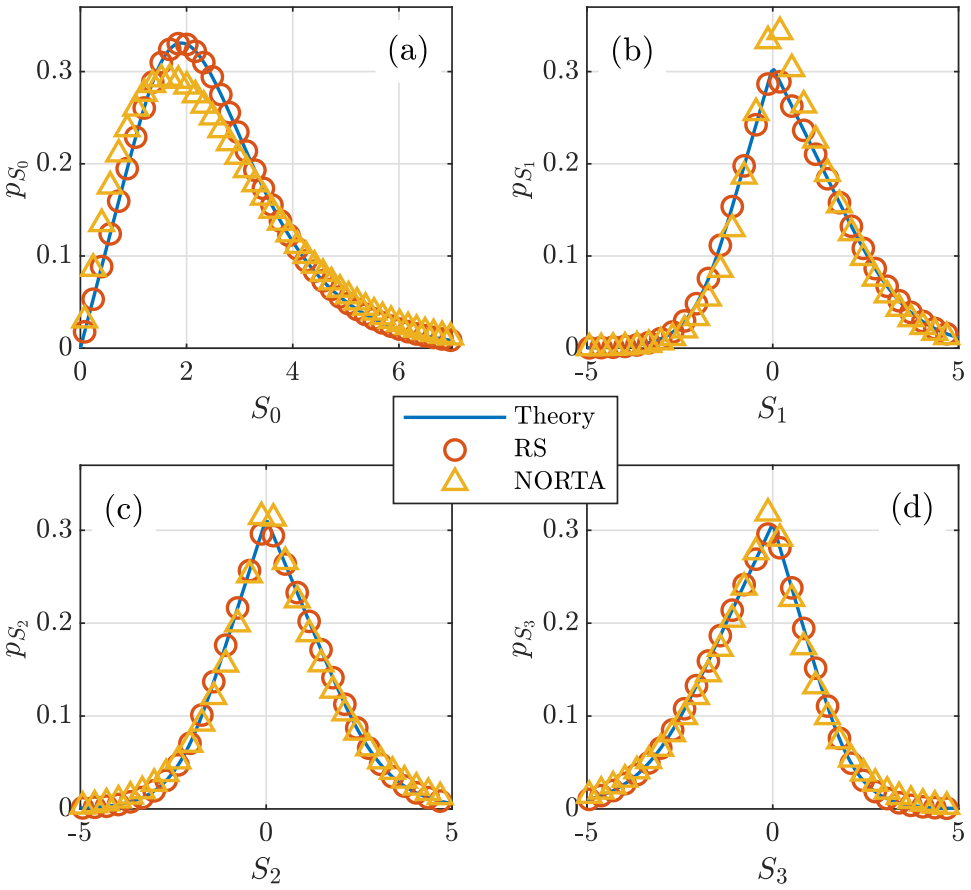

Figure 6. Stokes parameter PDFs: (**a**) p_{S_0}, (**b**) p_{S_1}, (**c**) p_{S_2}, and (**d**) p_{S_3}.

The results in Figures 4–6 clearly demonstrate the strengths and weaknesses of RS and NORTA algorithms for generating partially polarized MG fields. Although NORTA will not produce E_x and E_y with the proper joint PDF, if speckle size is critical to the application (or polarization is not a concern [24]), then NORTA is probably the best option. On the other hand, if the application demands accurate joint statistics, RS is likely the best choice.

4. Conclusions

In this paper, we generalized our prior work on stochastic scalar MG fields to the electromagnetic domain. We began with the derivation of the bivariate complex MG PDF, followed by the speckle contrast, and concluded the analysis with the instantaneous MG Stokes parameter PDFs. We found that the electromagnetic MG family admits tractable analytic formulas for the field moments, the speckle contrast, and the PDFs of the instantaneous Stokes parameters. Moreover, the range of the speckle contrast for electromagnetic MG fields is much larger than that of classic CCG fields, for a fixed state and degree of polarization.

We generated partially polarized MG speckle fields with a specified polarization matrix using the RS and NORTA methods to validate our analysis. The RS results matched the desired (theoretical) PDFs extremely well; however, the RS MG field realizations—E_x and E_y—were spatially delta-correlated and therefore, not representative of physical speckle patterns. The NORTA fields, on the other hand, had realistic (and controllable) speckle sizes, and the polarization matrix and marginal PDFs of E_x and E_y were extremely accurate. However, the NORTA E_x and E_y joint PDF did not agree with theory, resulting in discrepancies between the theoretical and simulated Stokes parameter PDFs and speckle contrasts. Future work on this topic will include trying to develop a hybrid RS-NORTA

method for generating partially polarized MG fields with controllable speckle sizes and accurate joint statistics.

Our calculations in this paper were applied to a specific MG PDF model based on a linear combination of circular Gaussian PDFs. However, by no means is the MG PDF limited to the circular Gaussian distribution and can be readily applied to other linear combinations of Gaussian functions, as long as the basic requirements for PDFs are satisfied.

Author Contributions: Conceptualization, M.W.H.IV and O.K.; formal analysis, M.W.H.IV and O.K.; investigation, M.W.H.IV; methodology, M.W.H.IV and O.K.; software, M.W.H.IV; validation, M.W.H.IV; visualization, M.W.H.IV and O.K.; writing—original draft preparation, M.W.H.IV; writing—review and editing, O.K. All authors have read and agreed to the published version of the manuscript.

Funding: O.K. acknowledges the support from the University of Miami under the Cooper Fellowship program.

Institutional Review Board Statement: Not applicable.

Informed Consent Statement: Not applicable.

Data Availability Statement: No new data were created or analyzed in this study. Data sharing is not applicable to this article.

Conflicts of Interest: The authors declare no conflict of interest. The funders had no role in the design of the study; in the collection, analyses, or interpretation of data; in the writing of the manuscript, or in the decision to publish the results.

Abbreviations

The following abbreviations are used in this manuscript:

MG	multi-Gaussian
PDF	probability density function
CCG	circular complex Gaussian
RS	rejection sampling
NORTA	normal to anything

References

1. Goodman, J. Some effects of target-induced scintillation on optical radar performance. *Proc. IEEE* **1965**, *53*, 1688–1700. [CrossRef]
2. Dainty, J. Some statistical properties of random speckle patterns in coherent and partially coherent illumination. *Opt. Acta* **1970**, *17*, 761–772. [CrossRef]
3. Goodman, J. Statistical properties of laser speckle patterns. In *Laser Speckle and Related Phenomena*; Topics in Applied Physics; Dainty, J.C., Ed.; Springer: Berlin/Heidelberg, Germany, 1975; Volume 9, pp. 9–75.
4. Dainty, J. The statistics of speckle patterns. In *Progress in Optics*; Wolf, E., Ed.; Elsevier: Amsterdam, The Netherlands, 1977; Volume 14, Chapter 1, pp. 1–46. [CrossRef]
5. Barakat, R. Statistics of the Stokes parameters. *J. Opt. Soc. Am. A* **1987**, *4*, 1256–1263. [CrossRef]
6. Brosseau, C.; Barakat, R.; Rockower, E. Statistics of the Stokes parameters for Gaussian distributed fields. *Opt. Commun.* **1991**, *82*, 204–208. [CrossRef]
7. Eliyahu, D. Vector statistics of correlated Gaussian fields. *Phys. Rev. E* **1993**, *47*, 2881–2892. [CrossRef] [PubMed]
8. Eliyahu, D. Statistics of Stokes variables for correlated Gaussian fields. *Phys. Rev. E* **1994**, *50*, 2381–2384. [CrossRef]
9. Brosseau, C. *Fundamentals of Polarized Light: A Statistical Optics Approach*; Wiley: New York, NY, USA, 1998.
10. Santalla del Rio, V.; Pidre Mosquera, J.M.; Isasa, M.V.; de Lorenzo, M.E. Statistics of the degree of polarization. *IEEE Trans. Antennas Propag.* **2006**, *54*, 2173–2175. [CrossRef]
11. Barakat, R. The statistical properties of partially polarized light. *Opt. Acta* **1985**, *32*, 295–312. [CrossRef]
12. Korotkova, O. Changes in statistics of the instantaneous Stokes parameters of a quasi-monochromatic electromagnetic beam on propagation. *Opt. Commun.* **2006**, *261*, 218–224. [CrossRef]
13. Chen, X.; Korotkova, O. Probability density functions of instantaneous Stokes parameters on weak scattering. *Opt. Commun.* **2017**, *400*, 1–8. [CrossRef]
14. Freund, I. '1001' correlations in random wave fields. *Waves Random Media* **1998**, *8*, 119–158. [CrossRef]
15. Dennis, M.R.; O'Holleran, K.; Padgett, M.J. Singular optics: Optical vortices and polarization singularities. In *Progress in Optics*; Wolf, E., Ed.; Elsevier: Amsterdam, The Netherlands, 2009; Volume 53, Chapter 5, pp. 293–363. [CrossRef]

16. Shinozuka, M.; Deodatis, G. Simulation of multi-dimensional Gaussian stochastic fields by spectral representation. *Appl. Mech. Rev.* **1996**, *49*, 29–53. [CrossRef]
17. Gbur, G.J. *Singular Optics*; CRC Press: Boca Raton, FL, USA, 2016.
18. Goodman, J.W. *Speckle Phenomena in Optics: Theory and Applications*, 2nd ed.; SPIE Press: Bellingham, WA, USA, 2020.
19. Raburn, W.S.; Gbur, G. Singularities of partially polarized vortex beams. *Front. Phys.* **2020**, *8*, 168. [CrossRef]
20. Korotkova, O.; Gbur, G. Applications of optical coherence theory. In *Progress in Optics*; Visser, T.D., Ed.; Elsevier: Amsterdam, The Netherlands, 2020; Volume 65, Chapter 4, pp. 43–104. [CrossRef]
21. Bender, N.; Yilmaz, H.; Bromberg, Y.; Cao, H. Customizing speckle intensity statistics. *Optica* **2018**, *5*, 595–600. [CrossRef]
22. Bender, N.; Sun, M.; Yilmaz, H.; Bewersdorf, J.; Cao, H. Circumventing the optical diffraction limit with customized speckles. *Optica* **2021**, *8*, 122–129. [CrossRef]
23. Bender, N.; Yilmaz, H.; Bromberg, Y.; Cao, H. Creating and controlling complex light. *APL Photonics* **2019**, *4*, 110806. [CrossRef]
24. Korotkova, O.; Hyde, M.W. Multi-Gaussian random variables for modeling optical phenomena. *Opt. Express* **2021**, *29*, 25771–25799. [CrossRef] [PubMed]
25. Wooding, R.A. The multivariate distribution of complex normal variables. *Biometrika* **1956**, *43*, 212–215. [CrossRef]
26. Goodman, N.R. Statistical analysis based on a certain multivariate complex Gaussian distribution (an introduction). *Ann. Math. Stat.* **1963**, *34*, 152–177. [CrossRef]
27. Wiener, N. Coherency matrices and quantum. *J. Math. Phys.* **1928**, *7*, 109–125. [CrossRef]
28. Wolf, E. Coherence properties of partially polarized electromagnetic radiation. *Il Nuovo Cimento* **1959**, *13*, 1165–1181. [CrossRef]
29. Born, M.; Wolf, E. *Principles of Optics: Electromagnetic Theory of Propagation, Interference and Diffraction of Light*, 7th ed.; Cambridge University Press: New York, NY, USA, 1999.
30. Mandel, L.; Wolf, E. *Optical Coherence and Quantum Optics*; Cambridge University Press: New York, NY, USA, 1995.
31. Goodman, J.W. *Statistical Optics*, 2nd ed.; Wiley: Hoboken, NJ, USA, 2015.
32. Richards, B.; Wolf, E.; Gabor, D. Electromagnetic diffraction in optical systems, II. Structure of the image field in an aplanatic system. *Proc. R. Soc. Lond. A* **1959**, *253*, 358–379. [CrossRef]
33. Novotny, L.; Hecht, B. *Principles of Nano-Optics*; Cambridge University Press: Cambridge, UK, 2006. [CrossRef]
34. Goldstein, D. *Polarized Light*, 3rd ed.; CRC Press: Boca Raton, FL, USA, 2011.
35. Korotkova, O. *Random Light Beams: Theory and Applications*; CRC Press: Boca Raton, FL, USA, 2014.
36. Picinbono, B. Second-order complex random vectors and normal distributions. *IEEE Trans. Signal Process.* **1996**, *44*, 2637–2640. [CrossRef]
37. Kalos, M.H.; Whitlock, P.A. *Monte Carlo Methods*, 2nd ed.; Wiley-VCH: Weinheim, Germany, 2008.
38. Grigoriu, M. Crossing of non-Gaussian translation processes. *J. Eng. Mech.* **1984**, *110*, 610—620. [CrossRef]
39. Yamazaki, F.; Shinozuka, M. Digital generation of non-Gaussian stochastic fields. *J. Eng. Mech.* **1988**, *114*, 1183–1197. [CrossRef]
40. Cario, M.C.; Nelson, B.L. *Modeling and Generating Random Vectors with Arbitrary Marginal Distributions and Correlation Matrix*; Tech. Rep.; Northwestern University: Evanston, IL, USA, 1997.
41. Yura, H.T.; Hanson, S.G. Digital simulation of an arbitrary stationary stochastic process by spectral representation. *J. Opt. Soc. Am. A* **2011**, *28*, 675–685. [CrossRef] [PubMed]
42. Yura, H.T.; Hanson, S.G. Digital simulation of two-dimensional random fields with arbitrary power spectra and non-Gaussian probability distribution functions. *Appl. Opt.* **2012**, *51*, C77–C83. [CrossRef]